ELSEVIER Nuclear Instruments and Methods in Physics Research B 136–138 (1998) 460–464

NIM B
Beam Interactions with Materials & Atoms

Nucleation and growth of platelet bubble structures in He implanted silicon

P.F.P. Fichtner [a,*], J.R. Kaschny [b], A. Kling [c], H. Trinkaus [d], R.A. Yankov [b], A. Mücklich [b], W. Skorupa [b], F.C. Zawislak [f], L. Amaral [f], M.F. da Silva [e], J.C. Soares [c]

[a] *Departamento de Metalurgia, Universidade Federal do Rio Grande do Sul, P.O. Box 15051, 91501-970 Porto Alegre, RS, Brazil*
[b] *Research Center Rossendorf, D-01314 Dresden, Germany*
[c] *Centro de Física Nuclear, Universidade de Lisboa, 1699 Lisboa, Portugal*
[d] *Institut für Festkörperforschung, KFA Jülich, P.O. Box 1913, D-5170 Jülich, Germany*
[e] *Instituto Tecnológico e Nuclear, 2685 Sacavém, Portugal*
[f] *Instituto de Física, Universidade Federal do Rio Grande do Sul, P.O. Box 15051, 91501-970 Porto Alegre, RS, Brazil*

Abstract

He^+ ions were implanted into (1 0 0) Si at energies from 30 to 120 keV and fluences from 5×10^{15} to 1×10^{16} cm^{-2}. After implantation, pieces of these samples were subjected to rapid thermal annealing for 600 s at temperatures ranging from 300°C to 700°C. The samples were analyzed by Transmission Electron Microscopy (TEM) and by Rutherford Backscattering and channeling spectrometry (RBS/C). The TEM observations were related to the RBS/C measurements and the results discussed in terms of a nucleation model to explain the formation of overpressurized bubbles in He implanted and annealed silicon. © 1998 Published by Elsevier Science B.V.

PACS: 61.72.C; 61.72.Q; 61.72.T; 61.82.V
Keywords: He bubbles; Defects; Ion implantation; Silicon

1. Introduction

The formation of implanted He induced cavities in single crystalline silicon is of present interest either in connection with the development of proximity gettering techniques for very large scale integration (VLSI) applications [1–3] or as an alternative tool for the production of silicon-on-insulator structures [4,5]. However, there have been relatively few systematic studies focusing the basic nucleation and growth phenomena of the He induced cavities in Si. In addition, most of these studies have concentrated only on the high dose implant cases (He fluences in the $\phi \geqslant 5 \times 10^{16}$ cm^{-2} range) where a high density of small bubbles (i.e., a condensed system) are produced during the implantation.

In order to improve the situation, we started a series of investigations with special emphasis placed on Si samples implanted with relatively

* Corresponding author. Fax: 55 (51) 3161762; e-mail: fichtner@if.ufrgs.br.

PII S0168-583X(97)00714-3

low doses where, after annealing, a rather low number of cavities are formed. Such structures are further referred to as diluted cavity systems in order to distinguish them from the above mentioned condensed ones. In particular, our preliminary results [6] have shown that each type of system presents quite a distinct cavity arrangement and morphology. Under similar annealing conditions (e.g. 600 s at 800°C), the condensed cavity systems are characterized by the formation of a dense array of cavities with diameters in the range of $1.8 \leqslant \phi \leqslant 18.5$ nm and located within the $R_p - \Delta R_p \leqslant x \leqslant R_p$ depth region, where R_p is the projected range and ΔR_p the range straggling of the He implant. The diameters of the cavities in the diluted systems were found to be in the range of $27 < \phi < 75$ nm and the cavities are located close to the R_p depth region. In addition, Transmission Electron Microscopy (TEM) observations have shown that the bubbles present a characteristic strain field contrast that, together with a calculation of their He content, support the concept that the cavities are He bubbles in an overpressurized state, rather than nearly gas empty cavities (i.e. voids) as predicted by first order gas release models [1,7,8].

In the present work we report combined results from TEM observations and RBS/C measurements which show new aspects of the bubble nucleation and growth behavior in such diluted bubble systems. These results may provide a better insight for a more general description of the He bubble nucleation and growth phenomena in single crystalline silicon.

2. Experimental procedure

In our experiments, (1 0 0) oriented CZ-Si wafers were implanted with He^+ ions at room temperature using energies and fluences of 40 keV and 1×10^{16} cm^{-2} (type **a**), or using three energies (30, 60 and 120 keV) and a fluence of 5×10^{15} cm^{-2} for each energy in order to form a flat-topped He concentration-depth profile (type **b**). After implantation, pieces of these samples were subjected to heat treatment for 600 s at temperatures ranging from 300°C to 700°C using a rapid thermal processing system. The 400°C and 500°C anneals of type **a** samples were analyzed by TEM to identify the microstructural features associated with the nucleation and growth of He bubbles. The TEM observations were performed in plan-view specimens thinned by ion milling. Type **b** samples were more systematically investigated by Rutherford Backscattering and channeling spectrometry (RBS/C) in order to study the crystal damage. The RBS/C experiments were carried out at the 3.1 MeV van de Graaff accelerator at Sacavém, using a 1.6 MeV He^+ beam. The backscattered particles were detected at an angle near 180° using an annular surface barrier detector with a resolution of 18 keV. Furthermore, in order to correlate the RBS/C measurements with the TEM observations, we also analyzed by TEM some pieces of type **b** samples annealed at 600°C and 700°C for 600 s.

3. Results and discussion

Fig. 1 shows a set of RBS/C spectra from samples of the type **b** corresponding to annealing temperatures of 350°C, 400°C and 470°C during 600 s. In order to provide a scale for the minimum and maximum damage levels Fig. 1 also presents the

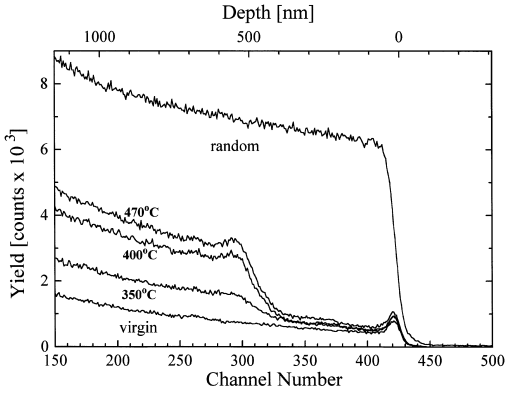

Fig. 1. RBS/C spectra from type **b** samples annealed at 350°C, 400°C and 470°C for 600 s. The spectra from an unimplanted (virgin) sample and the one from a sample oriented at a random direction provide a scale for the minimum and maximum damage levels detected in the RBS/C measurements. The scale on the top axis gives a depth profile for the measurements.

(1 0 0) aligned and random spectra from an unimplanted (virgin) specimen. For the depth region extending from the sample surface up to about 450 nm, the aligned spectra of the annealed specimens present a relatively low damage level. For larger depths, the same curves clearly show a dechanneling yield increasing with the temperature. The modifications are already clear at 300°C (not shown) and the maximum yield was observed to be around 470°C. For a temperature of 500°C (not shown) the backscattering yield is already slightly smaller than that of the 470°C spectrum and decreases significantly at higher temperatures ($T \geqslant 700$°C). The increase of the backscattering yield with increasing temperature in the range from 300°C to 470°C characterizes a reverse damage annealing behavior that should be correlated with the evolution of the microstructure caused by the He implantation.

Fig. 2 shows two TEM micrographs from a type **a** sample annealed at 400°C for 600 s. Fig. 2(a) presents a dynamic bright field multibeam image with the electron beam parallel to the ⟨1 0 0⟩ axis of the Si crystal. The image shows the strain fields around the He-filled structures with strong contrast. The morphology of the He-filled structures is only revealed in the bright field kinematic phase contrast images (underfocus) presented in Fig. 2(b). This micrograph clearly shows that the He-filled structures are not spherical, but, instead presents a platelet-like shape which can be observed either in their edge-on projections (see arrow) or in their face-on views. We remark that the phase contrast of the face-on platelets is quite weak due to the small thickness of the platelets compared to the large sample thickness, $t \approx 550$ nm, where these bubbles appear. We also remark that all the observed edge-on structures present their larger facets parallel to the (1 1 0) planes of the Si lattice. The diameters of these platelet bubble structures are in the range of 70–180 nm, and their corresponding thicknesses are about 3 nm. On the basis of the present observations, we assume that the (1 1 0) planes are the preferential ones for the nucleation of such platelet bubbles. Hence, the observed faces of the platelets should correspond to projected views from structures aligned in other available (1 1 0) planes. It is also

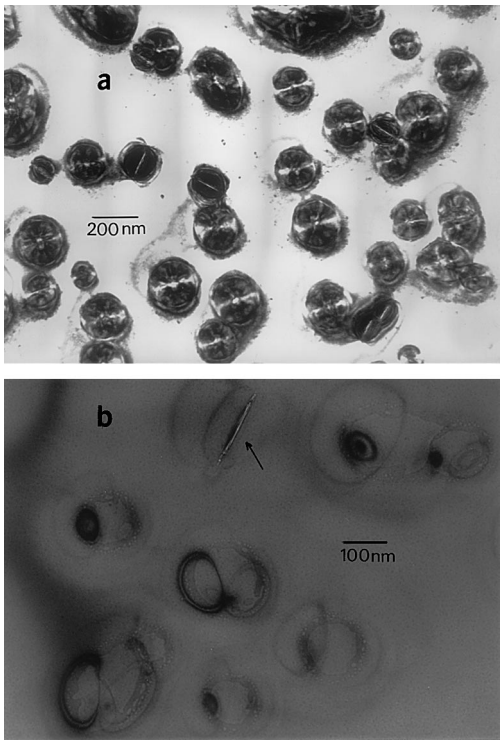

Fig. 2. Plan-view TEM micrographs showing a cavity system resulting from a 400°C, 600 s anneal of a type **a** sample. (a) Strain field contrast around the He-filled structures. Dynamic bright field multibeam image with electron beam parallel to the ⟨1 0 0⟩ axis of the Si lattice. (b) He-filled platelet structures imaged in their edge-on projections (see arrows) or in their face-on views. Kinematic bright field image, underfocus.

important to point out that most of the face-on platelet bubbles present a rather irregular shape resembling a "large island with capes and bays". These large islands are surrounded by a ring of "small islands" located close to the "coast".

Finally, TEM observations of samples annealed at higher temperatures show a distinct bubble morphology. For 500°C type **a**, and also for 600°C and 700°C (600 s) type **b** annealed samples, the bubble morphology can be characterized by the presence of a large and more spherical-like bubble surrounded by a ring containing a large quantity of smaller ones. This is shown in Fig. 3(a) for the case of a 700°C, 600 s, type **b** sample. The present data suggest that, upon thermal annealing at temperatures higher than 400°C, a transition oc-

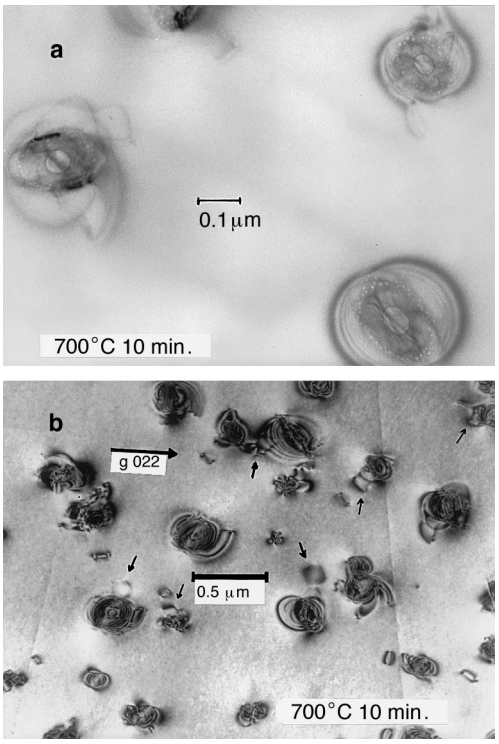

Fig. 3. Plan view TEM micrographs from type **b** samples. (a) Typical appearance of the bubble structures after thermal anneal above 400°C. Notice the large cavity surrounded by a ring containing a large number of smaller ones. Kinematic bright field image, underfocus. (b) Strain fields and dislocation loops emerging from the bubbles (arrows). Notice the presence of free dislocation loops in the matrix. Dynamic bright field two-beam image.

curs from the platelet-like morphology into a more spherical one. It is remarkable that the strong strain field contrast observed in the platelet structure is present in the higher temperature cases. Fig. 3(b) shows this situation for the same case shown in Fig. 3(a) (700°C, 600 s, type **b** sample). Together with the strain field contrast, the micrograph also shows dislocation loops emerging from the bubble structures (see arrows).

One can classify the nucleation and growth phenomena in He implanted and annealed Si in terms of three different regimes depending on the implanted He content [6]. The low He concentration regime is characterized by the formation of small He-vacancy (He_mV_n) clusters which may dissociate at rather low temperatures (e.g. $T \approx 250$°C), as discussed by Van Veen et al. [9]. The high He concentration regime is characterized by the formation of small bubbles during the implantation and leads to the condensed bubble systems characterized in Section 1. For the medium He concentration regime, we observed that the bubbles nucleate in a platelet structure that, upon thermal treatments at temperatures higher than 400°C, become overpressurized spherical-like bubbles surrounded by a ring containing a large number of smaller bubbles. It is difficult to explain the formation of such large and overpressurized bubbles using the existing bubble nucleation and growth concepts [10]. However, on the basis of the present data, we may propose an alternative description of the present observed phenomena. One can assume that some more stable He_mV_n clusters are formed and diffuse in the Si matrix already at rather low temperatures. Very probably these He_mV_n clusters can be trapped by other clusters or at lattice defects. As a consequence, the heterogeneous nucleation of platelet bubble structures occurs by the capture of other He_mV_n clusters. By increasing the platelet size, the large strain field produced in the matrix prevent the capture of new clusters by the main ''platelet-island''. Instead, it may favor the trapping of the incoming clusters in the strained lattice sites around the platelet, thus leading to the formation of the observed ring containing a large number of small bubbles. The platelet bubble structure may preserve the stable He_mV_n cluster properties, which may allow the formation of a large He-filled structure containing a rather high number of He atoms per vacancy. The morphological change from the platelet into the spherical like shape may also imply the transition from the He_mV_n cluster behavior into a real gas phase behavior, which indeed can lead to the overpressurized bubble formation.

On the other hand, the increase of the platelet sizes or their number density may lead to the increase of the dechanneling cross-section. Hence, the data in Fig. 1 can be correlated with the above He platelet bubble nucleation and growth process. The inclination of the Arrhenius plot obtained from the thermal behavior of the backscattering yield suggests that such microstructural evolution is governed by a single thermally activated

process with an apparent activation energy of about 0.37 eV.

4. Conclusions

We studied the nucleation and growth of He induced cavities with special emphasis placed on systems formed by rather low implanted He fluences, where large and overpressurized bubbles surrounded by strain fields and by a ring containing a large quantity of small bubbles can be observed. It was determined that such He bubble structures nucleate and grow by the formation of He-filled platelet structures which transform into a more spherical shape upon thermal annealing at temperatures higher than 400°C. This microstructural evolution was discussed in terms of the migration and coalescence of small He_mV_n clusters which are assumed to be rather mobile and stable at low temperatures.

References

[1] V. Raineri, P.G. Fallica, G. Percolla, A. Battaglia, M. Barbagallo, S.U. Campisano, J. Appl. Phys. 78 (1995) 3727.
[2] S.M. Myers, D.M. Follstaedt, J. Appl. Phys. 79 (1996) 1337.
[3] W. Skorupa, N. Hatzopoulos, R.A. Yankov, A.B. Danilin, Appl. Phys. Lett. 67 (1995) 7; R.A. Yankov, J.R. Kaschny, P.F.P. Fichtner, A. Mücklich, W. Skorupa, Microelectron. Eng. 36 (1997) 129.
[4] M. Bruel, Nucl. Instr. and Meth. B 108 (1996) 313.
[5] V. Raineri, S.U. Campisano, Appl. Phys. Lett. 66 (1995) 3654.
[6] P.F.P. Fichtner, J.R. Kaschny, R.A. Yankov, A. Mucklich, U. Kreißig, W. Skorupa, Appl. Phys. Lett. 70 (1997) 732.
[7] C.C. Griffioen, J.H. Evans, P.C. de Jong, A. van Veen, Nucl. Instr. and Meth. B 27 (1987) 417.
[8] S.M. Myers, D.M. Follstaedt, H.J. Stein, W.R. Wampler, Phys. Rev. B 47 (1993) 13380.
[9] A. Van Veen, H. Schut, R.A. Hakvoort, A. Fedorov, K.T. Westerduin, Mat. Res. Soc. Symp. 373 (1995) 499.
[10] H. Trinkaus, Radiat. Eff. 78 (1983) 189.